NASA TECHNICAL NOTE

NASA TN D-5166

c. 1

NASA TN D-5166

TECH LIBRARY KAFB, NM

0131969

LOAN COPY: RETURN TO
AFWL (WLIL-2)
KIRTLAND AFB, N MEX

INFRARED SPECTRAL IRRADIANCE MEASUREMENTS IN A SPACE ENVIRONMENT SIMULATOR

by John F. Rogers

Goddard Space Flight Center
Greenbelt, Md.

NATIONAL AERONAUTICS AND SPACE ADMINISTRATION • WASHINGTON, D. C. • JUNE 1969

TECH LIBRARY KAFB, NM

0131969

INFRARED SPECTRAL IRRADIANCE MEASUREMENTS IN A SPACE ENVIRONMENT SIMULATOR

By John F. Rogers

Goddard Space Flight Center
Greenbelt, Md.

NATIONAL AERONAUTICS AND SPACE ADMINISTRATION

For sale by the Clearinghouse for Federal Scientific and Technical Information
Springfield, Virginia 22151 – CFSTI price $3.00

ABSTRACT

An experimental program for measuring the infrared spectral irradiance from 2.9 to 29.3μ in the space environment simulator has been completed. During the series of measurements, the chamber was operated at full environmental conditions: solar simulation, liquid nitrogen conditioned walls, and a vacuum of 10^{-7} torr. Measurements were made with and without a spacecraft model in the chamber. Data are presented for the spectral irradiance and total irradiance as a function of instrument aspect angle, position in the chamber, solar simulator power variations, and spacecraft aspect angle. Results of the experiment indicate a collimated and a diffuse component of the radiation in the spectral range measured.

CONTENTS

Abstract ii

INTRODUCTION 1

DESCRIPTION OF THE SES AND THE MEASUREMENT PROGRAM 1

INSTRUMENTATION 4

Michelson Interferometer 4

Data Acquisition and Processing 7

Wavelength Calibration 9

Spectral Resolution 9

Energy Calibration 12

Field of View 13

RESULTS 14

Spectral Irradiance 14

Total Irradiance 17

Variations of Basic Infrared Model Caused by Changing of Chamber Parameters 21

CONCLUSIONS AND RECOMMENDATIONS 22

References 24

Appendix A—Nomenclature 25

Appendix B—Tolerances 27

INFRARED SPECTRAL IRRADIANCE MEASUREMENTS IN A SPACE ENVIRONMENT SIMULATOR

by
John F. Rogers
Goddard Space Flight Center

INTRODUCTION

The solar simulator beam radiates energy in the wavelength region of 0.28 to 2.5μ. In the thermal balance testing of a spacecraft, however, infrared energy being radiated by a solar simulator array in wavelengths longer than 2.5μ becomes important for spacecraft coatings which have a low solar absorptance and a corresponding high absorptance for the infrared energy. Thus for materials which exhibit these properties (white paint, alzak) it is necessary to know the infrared energy for accurate evaluation of the thermal test data. In the case of an α/ϵ (solar absorptance-thermal emittance) heater skin test for the Orbiting Astronomical Observatory (Reference 1), the solar test results indicated a higher α than predicted. The predicted α did not include the effect of infrared energy from the solar simulator array being incident onto the alzak skins. The series of measurements reported herein are for the purpose of defining the spectral irradiance, total irradiance, and spatial distribution of the infrared energy radiated from the solar array.

The use of standard infrared monochromators for the measurements presents serious problems because of the inaccessibility of the radiation, the low level of energy, the low efficiency of the monochromators, and the required spatial distribution of the radiation field. The application of interferometric techniques is especially suited to the problem because of the compactness of the units, high efficiency of light throughput, and the ability for direct installation of the spectrometers in the solar beam with only the electrical connections being needed.

DESCRIPTION OF THE SES AND THE MEASUREMENT PROGRAM

The space environment simulator (SES) is a large (27-foot diameter, 40-foot high clear volume inside the shroud), top loading vacuum chamber provided with liquid nitrogen cooled shrouds and a solar simulator. (Figure 1 shows an exterior view.) It is pumped by 17 32-inch oil diffusion pumps plus gaseous helium (20°K) cryopanels. The inner shroud may be flooded with liquid nitrogen (LN_2) during solar simulation tests or it may be conditioned with gaseous nitrogen from -65° to +85°C for either thermal-vacuum testing or for speeding up a return to ambient conditions from an LN_2 environment.

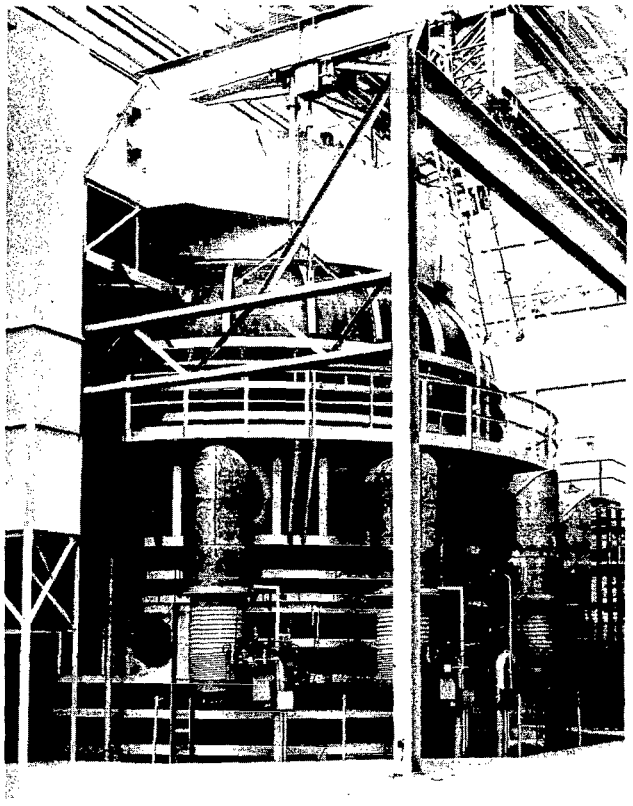

Figure 1—Exterior view of space environment simulator.

The solar simulator is contained in the top dome which can be rolled aside for loading. (An access door is also provided at the basement level.) The simulator is a modular system containing 127 replicate units. Figure 2 shows the basic design of a module.

Each module consists of a lamp (currently 3.5 kw mercury-xenon), whose energy is collected by an ellipsoidal reflector and focused through a series of condensing lenses to the chamber penetration point where a relay lens forms the chamber seal. The light transmitted through the relay lens falls upon a hyperbolic reflector where it is folded backward to a parabolic reflector and then reflected into the chamber volume. The parabola is hexagonally shaped so that the modules may be stacked.

The test volume uniformly illuminated by the simulator is roughly a right hexagonal cylinder 200 inches across corners and 20 feet high. A photograph of the solar array as seen from the test volume is shown in Figure 3.

There are two major sources that might contribute energy at wavelengths longer than 2.9μ to the test volume:

1. The arc electrode-envelope system of the 3.5 kw mercury-xenon lamp located external to the vacuum chamber emits infrared energy that must pass through four lenses of commercial grade fused silica. This energy follows optical paths

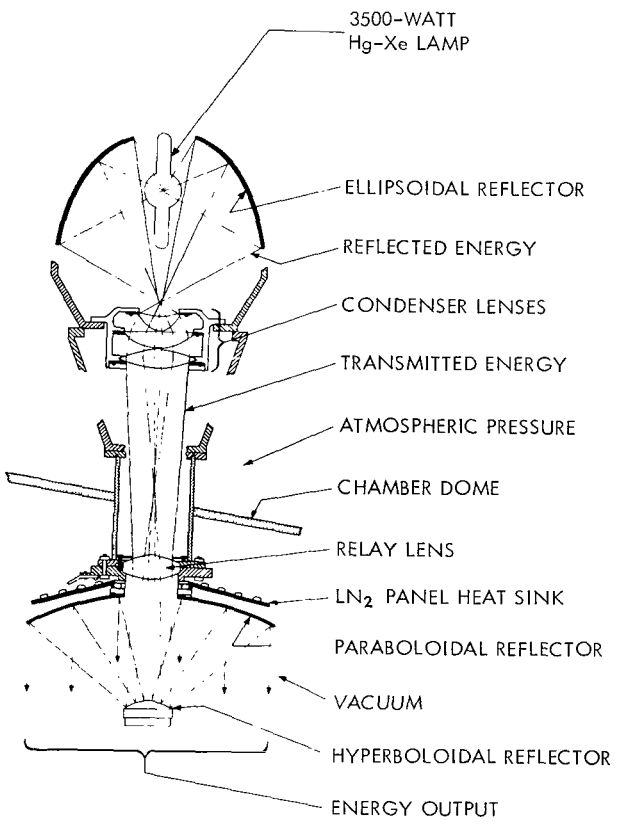

Figure 2—Basic design of solar simulator module.

similar to those of the direct solar simulator beam and is thus rendered "collimated" by the Cassegrain unit located within the vacuum chamber.

2. The relay lens, which is the last lens in the train, faces both the test volume and the hyperbolic reflector and would emit energy due to its temperature. Some of this energy will be collimated by the Cassegrain unit, and some will radiate directly to the test volume.

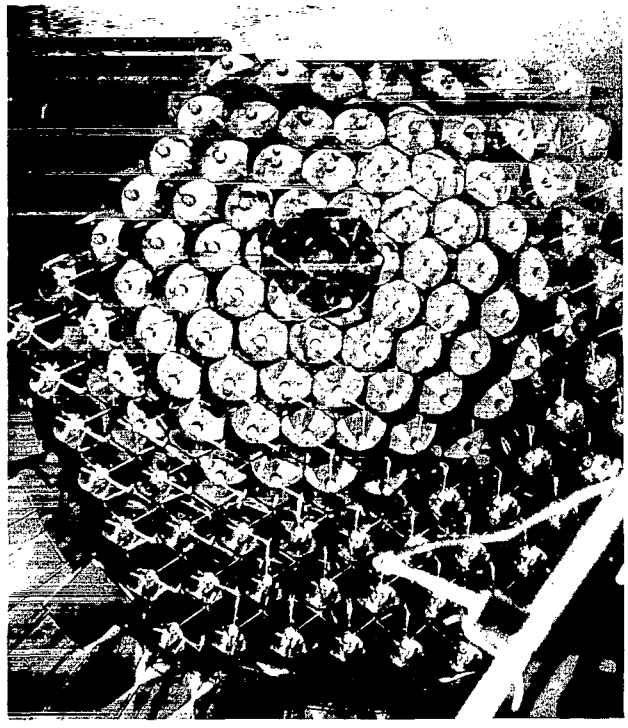

Figure 3—Photograph of solar array modules from test volume.

Miscellaneous secondary sources are the hyperbolic support structure, the parabolic support structure, spaces between the stacked parabolas, and the parabolic mirror.

The measurements were carried out in two phases of operation. For phase I, an OAO spacecraft model had been previously installed in the chamber for thermal evaluation. Figure 4 shows the location of the model with respect to the solar simulator modules. The model was relatively large and occupied a substantial portion of the useful solar beam, and the model surfaces exposed to the space environment were highly reflective. There was not sufficient time available during phase I to construct the instrumentation gimbals used during phase II. Since the instrumentation during phase I was aimed straight up at the solar array, a sun shade was installed on the north side of the chamber; interferometers could be located under the sun shade to prevent overheating. The associated electronics are shown schematically in Figure 4. The interferometers were installed on the radiation monitoring boom so that they could be moved into the shade when necessary.

The data taken during phase I were obtained under the following conditions:

Height: 19-foot level

Positions: under heating modules 33, 99, 65

Solar intensities: 0.83 and 0.65 solar constants

Model orientation: 85°W, 55°W, 0°W

The second phase was a program designated specifically for spectral measurements in the chamber. The empty chamber was made available in order to obtain data on depth of field of the solar beam. The heaters installed on the instruments were the same as during phase I. The shutter

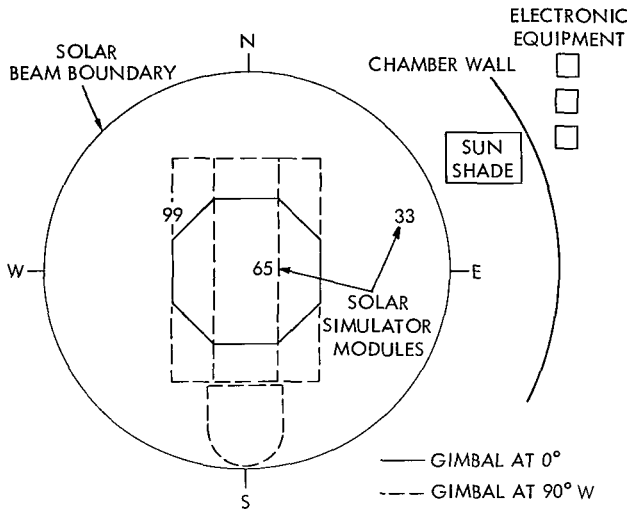

Figure 4—Spacecraft model location relative to modules.

systems were such that a constant temperature surface could be viewed by the interferometers with the solar simulator on or off. They were also constructed so as not to interfere with the field of view of the instruments while chamber measurements were being made. The plan was to expose the instruments to the solar beam for a 2-minute data acquisition period, thus avoiding heating effects on the interferometers. The gimbal on which the interferometers were mounted was constructed from miscellaneous hardware available in the laboratory. The angular position of the instruments was determined by relating the tilt angle to a voltage reading of a 10-turn potentiometer. The potentiometer was mounted on the side of the gimbal and shielded from the solar simulator to avoid heating effects. Because of the additional structure, the mounting position of the hardware could not be the same as that of phase I. The data taken during phase II were obtained under the following conditions:

Height: 19, 25, and 31 feet

Positions: under heating modules 32, 65, 107

Solar intensity: 0.83 and 0 solar constants

Instrument tilt(s): 0° to 20°

The number of spectral scans thus obtained totaled 180. It was felt that any further mapping of the chamber for detailed definition of the radiation field would result in an excessively large volume of data.

INSTRUMENTATION

The Michelson Interferometer

The essential feature of the formation of fringes in a parallel plate interferometer is the division of a beam of light by partial reflection and subsequent superposition of the two beams after they have traveled unequal optical paths. The incoming beam I_0 (Figure 5a) is divided at point S into two beams of equal intensity by the half silvered* rear surface of the substrate plate. The beams are reflected at the front-aluminized mirrors M_m and M_s and recombine at point S. The uncoated compensator plate is identical to the substrate plate; it is used so that the separate beams have equal paths in glass, which is necessary when white light fringes are to be observed. M_{mv} is

*The plate S is cesium iodide while the reflecting material is germanium for the far IR instrument; plate S is Nacl with a germanium reflective surface for the near IR instrument.

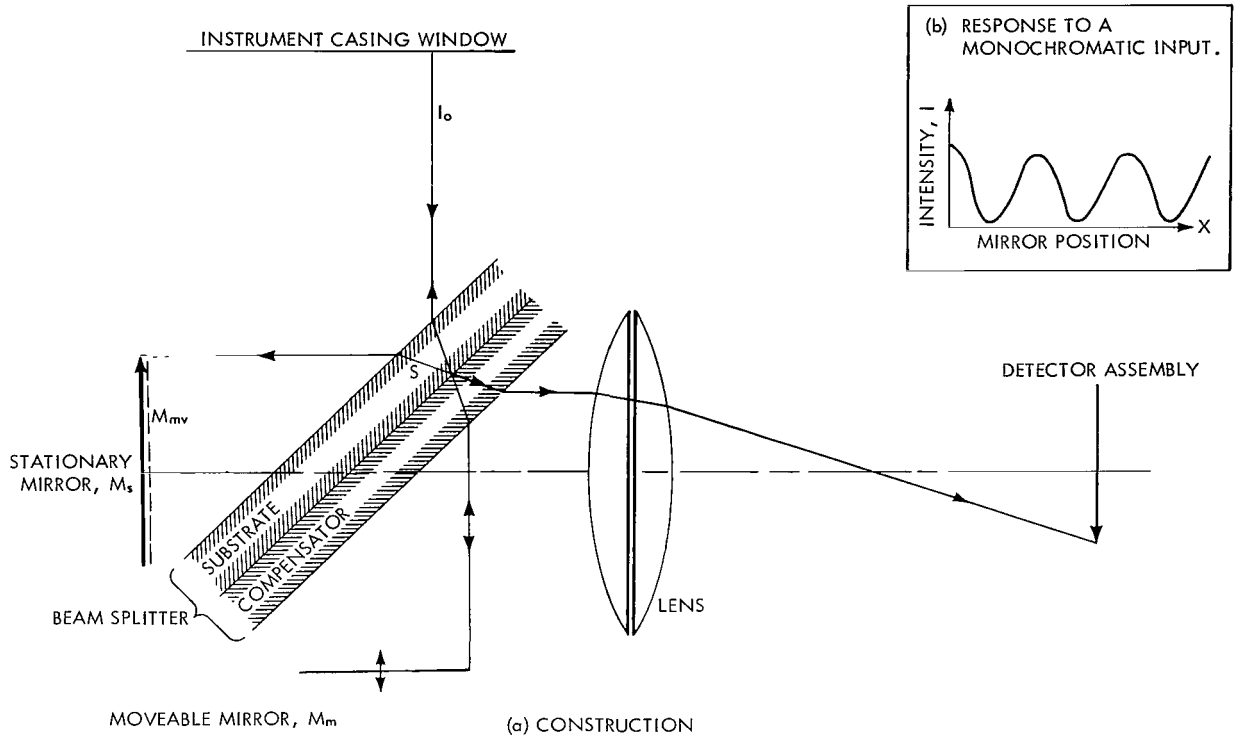

Figure 5—Construction and response of the Michelson interferometer optical cube.

the virtual image of M_m, formed by reflection at the point S; any beam that has undergone reflection at M_m behaves exactly the same as if reflected by a hypothetical mirror located at M_{mv} (Reference 2). That is, if moveable mirror M_m is adjusted so that M_m and M_s are perpendicular, and so that distances SM_m and SM_s are slightly different, then fringes at the detector are similar to those of a parallel-plate interferometer where the source, plates and detector, lie on the same axis. Hence, with an extended source, the fringes are concentric fringes of equal inclination. The lens shown in Figure 5a forms an image of M_s at the detector assembly (shown as the inverted arrow in the figure). The transfer function from M_s to the instrument casing window is one, and hence the limiting entrance aperture, when no foreoptics are used, is M_s.

If a monochromatic source of frequency ν is incident on the interferometer, the form of the intensity $I(x)$ measured by the detector, as M_m is moved from zero path difference, is

$$I(x) = I_0 \cos(2\pi\nu x) \tag{1}$$

where x, the path difference, is twice the mirror displacement (Reference 3). This intensity measurement is referred to as the interferogram. Any spectrum $B(\nu)$ can be considered to be an assembly of monochromatic lines, and the corresponding interferogram will be a linear superposition

of curves like that in Figure 5b and will have the form,

$$I(x) = \int_{-\infty}^{+\infty} B(\nu) \cos(2\pi\nu x)\, d\nu \ . \tag{2}$$

The variables of frequency, ν, and path difference, x, are conjugate variables, and an inversion can be made by Fourier's integral theorem to obtain an expression for the intensity as a function of frequency in terms of the intensity ordinates of the interferogram,

$$B(\nu) = \int_{-\infty}^{+\infty} I(x) \cos(2\pi\nu x)\, dx \ . \tag{3}$$

This relationship is the basis of Fourier spectroscopy and digital computers are used to make the numerical calculations to transform the information in the observed quantities into the required spectral elements (Reference 4).

The assignment of a finite upper limit to Equation 3 is primarily determined by the spectral resolution, $\Delta\nu$, required of the experiment, which in turn defines a number of frequency elements, $N = [\nu_1 - \nu_2]/\Delta\nu$, in the spectrum. The upper limit of the integral may be replaced by x, the maximum path difference; and assuming a symmetrical interferogram about zero path difference, Equation 3 becomes

$$B(\nu) = 2 \int_{0}^{x} I(x) \cos(2\pi\nu x)\, dx \ . \tag{4}$$

In some applications the experimental interferograms are not symmetric about zero path difference and the analysis can no longer be done by the transform using only cosine terms; the sine terms must also be included (Reference 3) so that the general interferogram has the form

$$I(x) = \int_{-\infty}^{+\infty} B(\nu) \cos(2\pi\nu x)\, d\nu + \int_{-\infty}^{+\infty} B(\nu) \sin(2\pi\nu x)\, d\nu \ , \tag{5}$$

and the spectrum

$$P(\nu) = \int_{-\infty}^{+\infty} I(x) \cos(2\pi\nu x)\, dx \ , \tag{6a}$$

$$Q(\nu) = \int_{-\infty}^{+\infty} I(x) \sin(2\pi\nu x)\, dx \ . \tag{6b}$$

In terms of these quantities, the energy spectrum is given by

$$B = \left(P^2 + Q^2\right)^{1/2} , \qquad (7)$$

which must be determined in obtaining energy spectra with an unavoidable phase shift characteristic. In this case the interferogram must be recorded from $-x$ to $+x$.

The construction of both near and far IR interferometers is basically the same (Figure 6). The Michelson interferometer (MI) is of cube type construction in which the optical paths have been bored through the solid aluminum. A tilt adjustment is accomplished by a ball and socket mount for the stationary mirror, and a translation adjustment is made by sliding the two halves of the cube along the diagonal. The motion of the moving mirror is obtained by mounting it on a loudspeaker type transducer that has no alignment adjustments. The cube is contained within the cylindrical housing which provides a vacuum-rated enclosure. A preamplifier and a high voltage supply for the detector are also in the optical head to lessen signal attenuation and stray noise pickup.

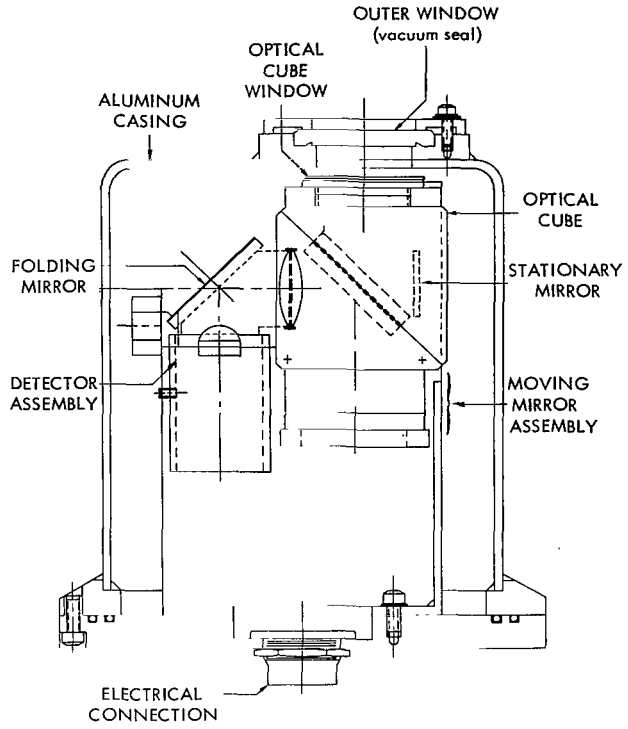

Figure 6—Mechanical arrangement of the interferometer.

Data Acquisition and Processing

A flow chart summarizing data acquisition and subsequent processing is given in Figure 7. The chamber interface is shown at the left side of the figure with the inputs to the various control units. The electronic units for the interferometers contain necessary post amplifiers for the intensity signal and sweep positions of the moving mirror, control units for the heater circuit used to maintain the detector assembly at a constant temperature of 37°C, the sweep time and sweep length selection of the moving mirror, and the attenuation circuit for the voltage level of the interferogram. The usable outputs of these control units are the interferogram itself, the sync pulse that triggers and A/D conversion at the beginning of each new interferogram, and a box car pulse that specifies the length of the interferogram. The sync pulse and box car pulse are recorded on one channel of the FM tape recorder, while the interferogram is recorded simultaneously by the recorder on a separate channel. These outputs are monitored by a scope before and after the FM recorder. Heaters were placed on the casing of the interferometers to maintain the units at 25°C, with the resulting temperatures being monitored to ensure that 25°C was maintained regardless of the operating mode of the units. For example, when the units were tilted at 10° to the normal, the amount of heat supplied to the units was reduced because of the exposure of the units to the solar

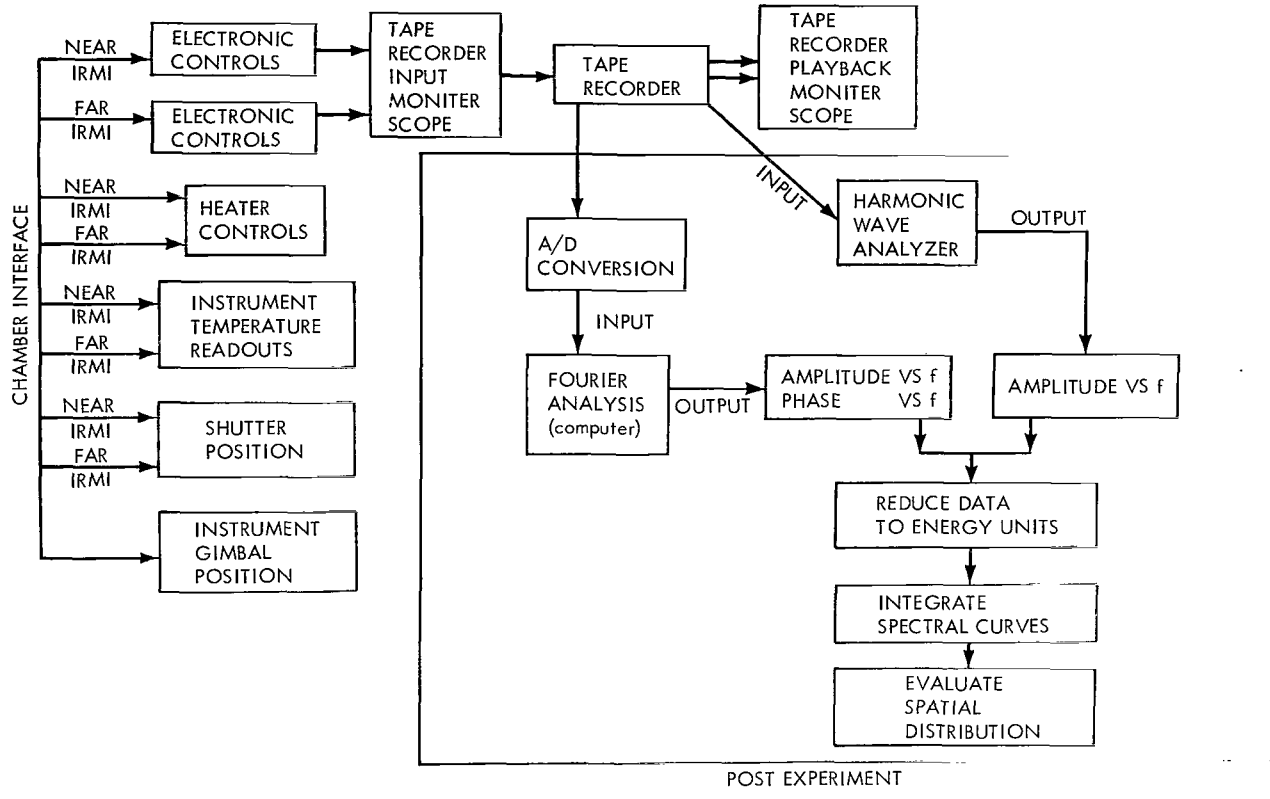

Figure 7—Data acquisition and processing flow chart.

beam. Similar heaters and controls were placed on the shutter system so that the shutter facing the interferometer was maintained at a constant temperature. The shutter system was always closed except for the 2-minute data acquisition period, thus maintaining the unit at a constant 25°C.

The information available to the experimenter consists entirely of the interferogram. Visual interpretation of this information with regard to the incident spectrum is virtually impossible; there is considerable time delay before an amplitude spectrum can be made available. Additionally, interpretation of the amplitude spectrum relative to the reduced spectrum is complicated by both instrument responsivity, which greatly modifies the record, and phase angle or energy reversals as explained further. Thus the experimenter obtains vast quantities of data with no real-time knowledge of the data's validity.

The subsequent data processing can now take one of two paths: either through the digital computer, which is extremely accurate and from which phase angle information is available; or through the harmonic wave analyzer, which can be faster and simpler but from which no phase angle information is available. The digital computer path is that of A/D conversion, co-adding a number of interferograms to eliminate noise, followed by Fourier analysis. The information obtained is thus the amplitude spectrum (the voltage at the computed frequencies) and the phase angle at the same frequencies. When using the wave analyzer, optimum conditions exist when the analyzer bandwidth

is approximately equal to the sweep frequency of the moving mirror, i.e., when the bandwidth = sweep frequency = 1/T, where T is the sweep time. For this application 1/T = 1.7 Hz, while the band pass filter was 2 Hz. A cyclic variation in the output record could be produced when the bandwidth of the wave analyzer does not match or exceed the sweep frequency which could then be interpreted as "fine" structure. Also, if the band pass filter exceeds the sweep frequency, resolution as available from the instrument will be lost and determined on the basis of filter bandwidth. The use of the wave analyzer offers rapidity when a large volume of data is to be processed. It was especially applicable for this experiment because of the absence of absorption and/or emission lines. The data were initially processed by the digital computer; subsequently, after a suitable filter arrived and was calibrated, the wave analyzer was employed.

Wavelength Calibration

The interferometers produce an output that is linear in wave number versus frequency; therefore, the wavelength calibration consists simply of finding the slope of this line knowing that it starts at the origin. The calibration experiment consists of placing a polystyrene filter with known absorption bands between the source and the interferometer and identifying the known bands on the frequency scale of the resulting spectrum. The experiment was performed using both the computer-adapted data reduction system and the wave analyzer before and after the measurement program, with and without the tape recorder. The location of the absorption bands for all the experiments remained at the same frequency; i.e., there was no observable degradation of the drive mechanism of the interferometers during this short time period, nor did the tape recorder measurably reduce the accuracy of the wavelength calibration.

The resolution of the instrument in this application was a function of maximum path difference and is theoretically 15 cm^{-1}. In practice, the resolution is generally at least twice this, or 30 cm^{-1}. The approximate resolution is helpful when correlating the observed spectrum of the polystyrene filter with that as measured by an IR spectroradiometer (in this case a Beckman IR 9). Figure 8 presents the absorption characteristics of the polystyrene filter used for both data reduction techniques. The first identifiable absorption band occurs at 540 cm^{-1} and is sufficiently wide and isolated from other bands as to be easily recognizable. The next bands occur at 700 cm^{-1} and 760 cm^{-1}, and these two appear as a single band on the interferometer reduced spectrum. The estimated wave number used was simply the average or 730 cm^{-1}. The remaining wave numbers versus frequencies given in Table 1 were similarly deduced.

Spectral Resolution

The criteria for spectral resolution for the experiment was not set by any of the instrument parameters, but rather by the nature of the environment in which the measurements were made and the nature of the signal from the interferometer due to incident energy from the solar array. The mercury-xenon lamps are dc powered from a silicon rectified power supply. There is a 3 percent ripple as measured at the power supply which, unfortunately, is transferred to the solar output beam as noise. This noise appeared in the interferogram, and its elimination necessitated

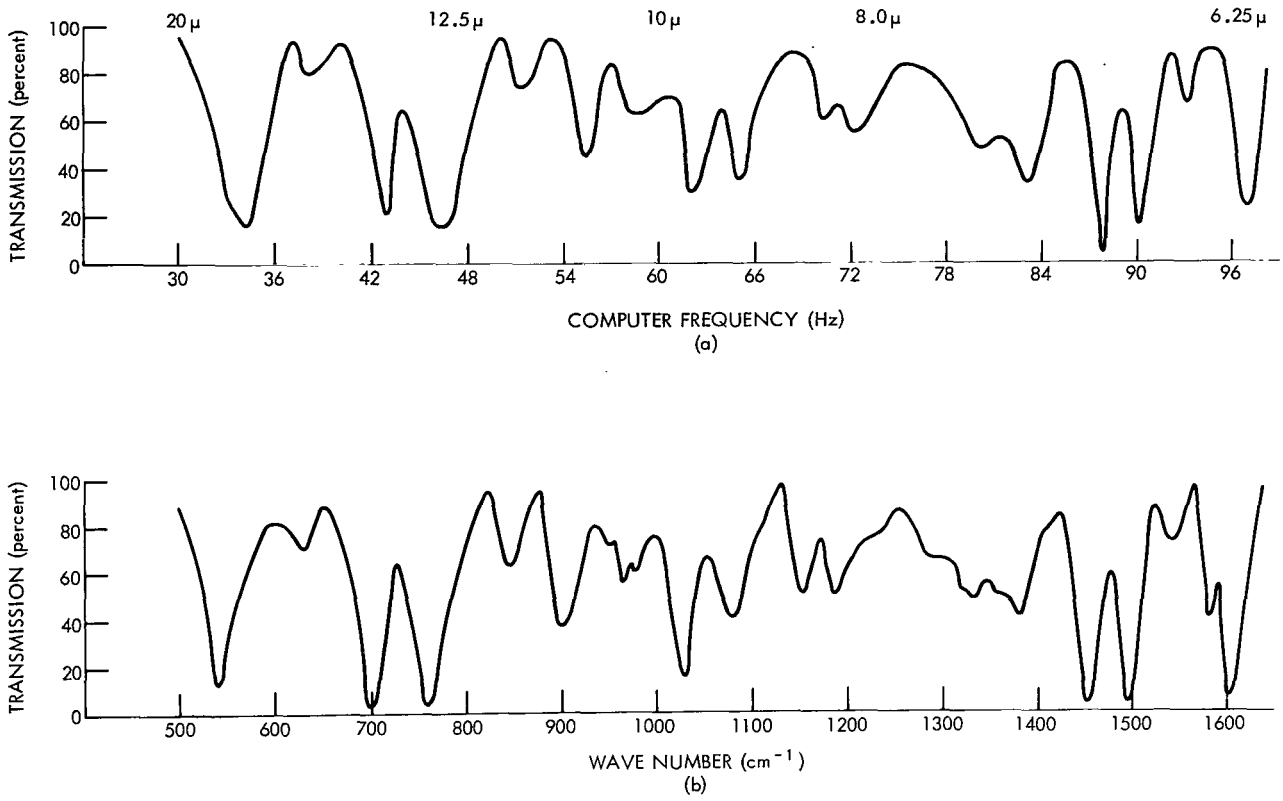

Figure 8—Absorption spectra of the polystyrene filter, (a) observed on far IR interferometer (X_0 = 666μ) and (b) measured with Beckman spectrophotometer IR 9.

Table 1

Wavelength Calibration.

λ (μ)	ν (cm^{-1})	f Computer (Hz)	f′ Wave Analyzer	f/ν Computer	f′/ν Wave Analyzer
18.5	540	16	62	2963	1130
13.7	730	21	84	2877	1151
10.8	930	-	102	--	1102
9.43	1060	30	120	2830	1132
8.58	1165	34	132	2918	1133
7.30	1370	39	151	2847	1102
6.80	1470	43	165	2924 (2893)	1122 (1125)

co-adding 50 scans. In addition, it was desirable to obtain the scans in a short time to avoid heating effects at the interferometer. Finally, the link from the analog tape to the final A/D tape collected at the computer complex is by voice control and requires more scans in the analog tape than can be collected. The sweep time selected arbitrarily for the moving mirror was 0.4 second with the corresponding sweep length of 333μ.

The spectral resolution for the instrument operated without any fore optics is given in Figure 9. The resolving power of a spectrometer is generally specified by $R = \nu/\Delta\nu$. The resolving power of the interferometer is calculated from either

$$R = \nu x_0 \tag{8a}$$

or

$$R = \frac{1}{\gamma^2}, \tag{8b}$$

whichever is smaller. The resolving power is limited by the maximum path difference (Equation 8a) or by obliquity effects (Equation 8b). The instrument design criteria used by the manufacturer of the instruments was such that the resolution would be determined by the path length difference rather than obliquity limitations, as seen in Figure 9.

A separate experiment had been run using a black body (small aperture with no obliquity effects) and the polystyrene filter to determine how many of the absorption bands could be resolved at the maximum sweep length setting of 666μ mirror motion. The ratio of the filtered spectrum to the unfiltered spectrum was taken and is given in Figure 8. An estimate of the resolution is 25 cm^{-1} based on the width of the 1155 cm^{-1} band. In general the resolution obtainable is twice that calculated and should be in the order of 15 cm^{-1}. The extremely narrow band of 10 cm^{-1} at 1580 cm^{-1} is not resolved, but it is possible that a resolution of better than the measured 25 cm^{-1} can be obtained. The 25 cm^{-1} resolution found here compares with the 60 cm^{-1} found in the section under wavelength calibration and is due to the 666μ mirror motion versus the 333μ.

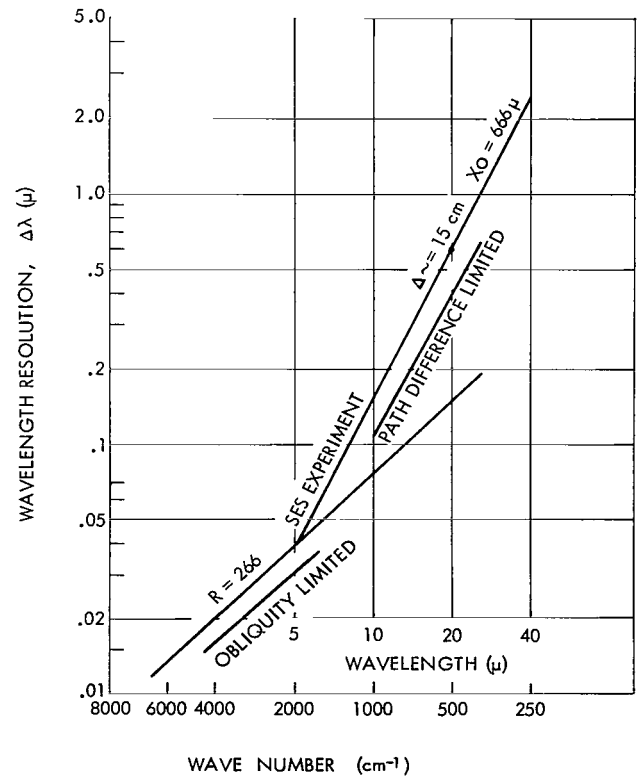

Figure 9—Theoretical spectral resolution.

Energy Calibration

Spectral Irradiance—Procedure

In order to obtain absolute irradiance values while looking at an unknown source, it is necessary first to determine the spectral radiant responsivity of the spectrometer because the output signal from the spectrometer is proportional to the differential irradiance between the source and some known reference such as the detector itself. Thus for a given wave number

$$Re_\nu = \frac{V_{1\nu}}{\Delta N_\nu} = \frac{V_{1\nu}}{(N_{\nu s} - N_{\nu B})}, \tag{9}$$

where $V_{1\nu}$ is the output voltage, Re_ν is the spectral radiant responsivity, $N_{\nu B}$ is the spectral irradiance of the detector, and $N_{\nu s}$ is the spectral radiance of the source.

The spectral responsivity calibration consists of measuring the output voltage with various spectral radiances of the source at different wave numbers throughout the spectrum. The relation between $V_{1\nu}$ and $N_{\nu s}$ is represented by a straight line of slope Re_ν that intercepts the $N_{\nu s}$ axis at $N_{\nu s} = N_{\nu B}$. In the calibration, $N_{\nu s}$ is the radiance of a variable-temperature black body source. By this method, Re_ν and $N_{\nu B}$ are determined as a function of wave number.

The unknown source for this application of the interferometer spectrometer was such that the field of view of the instrument was always filled. The calibration of the instrument, then, was performed in a similar fashion; i.e., the field of view was contained within the bounds of the source. The measurement of the spectral irradiance of the unknown source was accomplished in a vacuum environment so that the calibration was again similarly performed in the vacuum environment.

The spectral irradiance, $N_{\nu s}$, of the unknown source is a double-valued function of the observed quantity V_ν related to the calibration parameters $N_{\nu B}$, Re_ν by

$$N_{\nu s} = N_{\nu B} \pm \frac{V_\nu}{Re_\nu}, \tag{10}$$

where the plus sign is appropriate for sources more intense at wavelength ν than the detector, and the minus sign applies for sources less intense than the detector. The detector in the instrument is maintained at a constant temperature of 37°C so that in this measurement the net radiant flux could be in either direction. Normally the detector temperature is maintained so that no reversal occurs; however, since the quantity of energy was completely unknown, it was not possible to achieve the condition of no reversals. The phase angle information from the digital computer reduction indicates when a phase reversal occurs (i.e., a 180° abrupt change.) Thus given prior knowledge as to which phase angle indicates net outgoing or incoming radiance, the proper sign to be applied at any wave number may be determined.

Spectral Irradiance—Experimental Results

The entire apparatus used for the SES measurement program was transferred to a smaller vacuum chamber equipped with liquid nitrogen walls. The calibration sources were placed 6 inches from the front windows of the interferometers. The instruments and shield were maintained at the same temperatures as experienced in the SES. The temperatures selected for the sources were 10°, 50°, 95°, and 150°C. The lowest temperature of 10°C was used to obtain data points for the far IRMI for which preliminary data reduction had revealed phase reversals at the longer wavelengths. The series of measurements were recorded on tape in exactly the same way as the data obtained from the SES.

The curves representing Re_ν are shown in Figure 10 for both instruments. The spectral region where both instruments respond to the irradiation is from 5.0μ to 12.0μ. For wavelengths greater than 29.2μ, the data from the far IRMI become marginal since the sensitivity of the instrument decreases rapidly, and the incident energy similarly decreases. The sensitivity of the near IRMI decreases at wavelengths shorter than 3.0μ; however, there is significant energy at wavelengths shorter than 3.0μ from the SES solar array. Therefore it is desirable to extend the calibration to as short a wavelength as feasible.

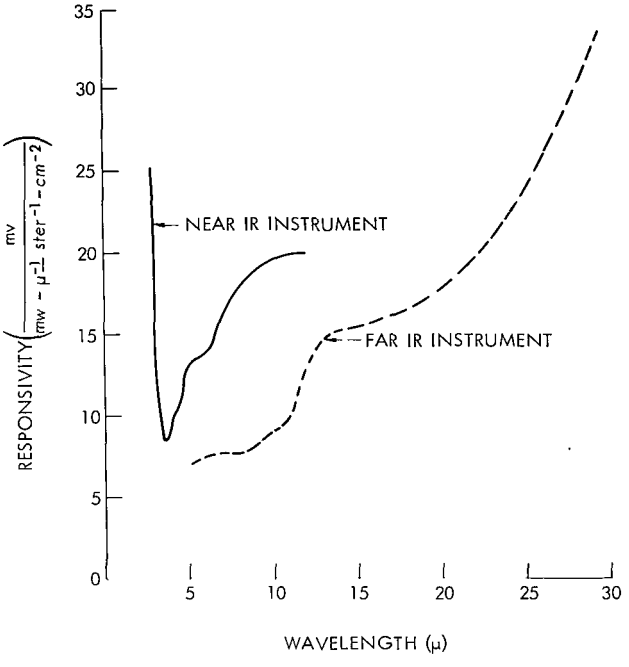

Figure 10—Spectral responsivity.

The shortest wavelength at which the calibration data from the original experiment were valid was 2.9μ. An attempt was made to use a higher temperature black body that did not fill the field of view to calibrate the short wavelengths. The results were rejected when no correlation could be found for the responsivity computed when compared to the original responsivity shown in Figure 10. Two reasons for the non-applicability are that the black body did not fill the field of view and that the second calibration was performed under room conditions and not in the vacuum environment. Therefore, some useful data taken at the shorter wavelengths in the SES, were lost because of lack of calibration data.

Field of View

The field of view was determined by placing the interferometers on an indexing head at a sufficient distance from a black body cavity so that the angular subtense of the black body was small. The distance was 140 cm and the aperture of the black body 0.92 cm so that the half-angle of the black body at the interferometer was 11 minutes. The center of the front window of the interferometer

was aligned with the center of the black body cavity at the different orientations of the interferometer. The interferometers were rotated in 1 degree increments using the front window axis as the axis of rotation. The black body was operated at a number of different temperatures at the 0 degree position. The calibration procedure of the preceding section was repeated using the temperature data obtained in this manner. Having obtained $N_{\nu s}$ and Re_{ν} for this experimental arrangement, the field of view of the instrument could be determined for the data analysis system used, i.e., the wave analyzer system. The field of view is given in Figure 11 for the far IRMI instrument for wavelengths of 5.0, 7.3, and 13.2μ. An average value of all the wavelengths studied was used for the field of view.

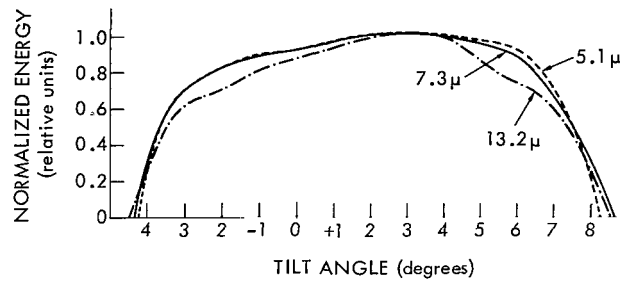

Figure 11—Field of view; far IRMI.

RESULTS

The method of presenting the data obtained from the measurement program outlined earlier is that of developing a basic infrared model of the solar array for the empty chamber and then evaluating the variations to be expected from the basic model due to experimental changes of chamber operation. The following discussion concerns the spectral irradiance and total irradiance values in terms of the field of view of the instruments and the total irradiance values in terms of a unit test item viewing the entire solar array.

Spectral Irradiance

To summarize the procedure used to obtain the spectral irradiance, the interferogram was transformed to an amplitude spectrum (voltage vs frequency) and reduced to a spectral irradiance curve using the responsivity, detector assembly irradiance, and the emissivity of the black paint on the calibrating source. An example of the amplitude spectrum is shown in Figure 12 for the far IRMI and in Figure 13 for the near IRMI. The usable spectral region of the far IRMI was judged to be from 5.0 to 29.3μ. At 29.3μ the sensitivity of the instrument drops rapidly, making energy values beyond 29.3μ uncertain. Region I of

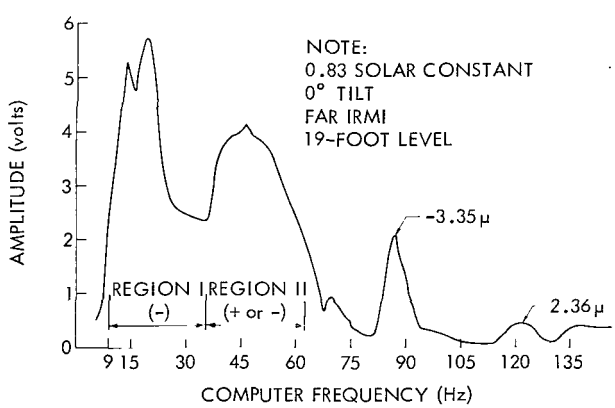

Figure 12—Amplitude spectrum; far IRMI.

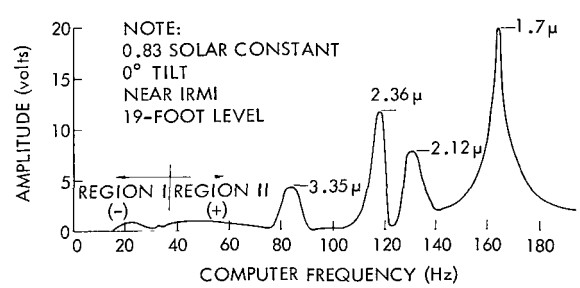

Figure 13—Amplitude spectrum; near IRMI.

Figure 12 is the band of net outgoing energy, except at the high tilt angles for which Region II becomes net out also. At the high tilt angles, the bands at 2.36 and 3.35μ (Figure 12) disappear, which means simply that those bands are no longer contained within the field of view of the instruments. The data obtained from the near IR instrument (Figure 13) were extremely limited. Most of the energy measured by the instrument was outside the available calibration range as the energy is concentrated in the 1.7, 2.12, 2.36, and 3.35μ spectral bands. The data used from the near IRMI were limited to the spectral region of 2.9 and 5.0μ.

The detector irradiance was obtained by the method outlined under the heading "Energy Calibration," as well as by viewing liquid nitrogen cooled walls during the measurement program. The

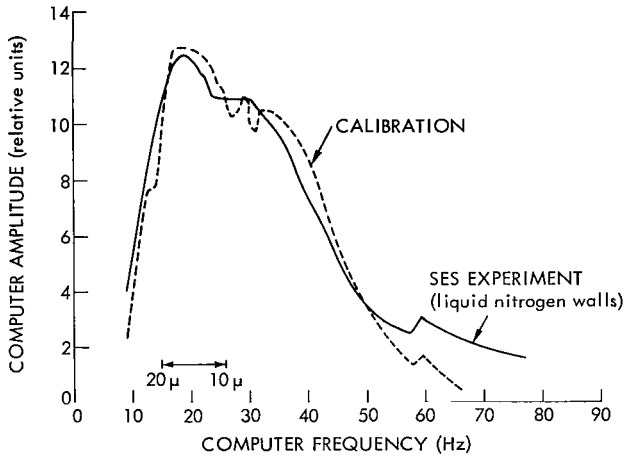

Figure 14—Amplitude spectra; detector far IRMI.

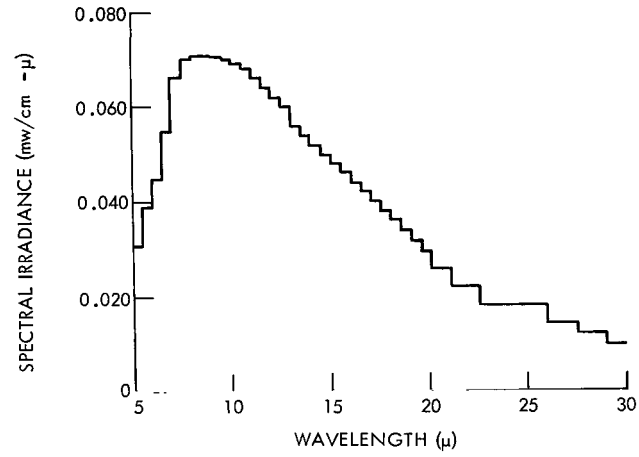

Figure 15—Detector spectral irradiance for far IRMI.

amplitude spectra obtained by both methods are shown in Figure 14. The correlation of the data was surprisingly good, with the largest uncertainty appearing at the shorter wavelengths where the energy values become very small. The final detector irradiance used is shown in Figure 15 using absolute energy values of mw/cm^2 μ.

The spectral irradiance curves obtained for all the measurements were very similar and are characteristically shown in Figures 16 to 19. The experimental conditions are as noted on the figures. The notable feature of the spectra obtained was the absence of absorption bands in the 5 to 29.3μ region. The initial data reduction was accomplished using all of the

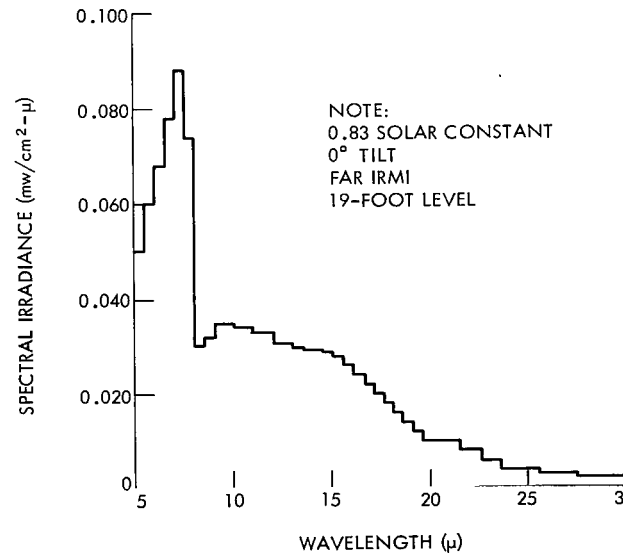

Figure 16—Spectral irradiance under module 64.

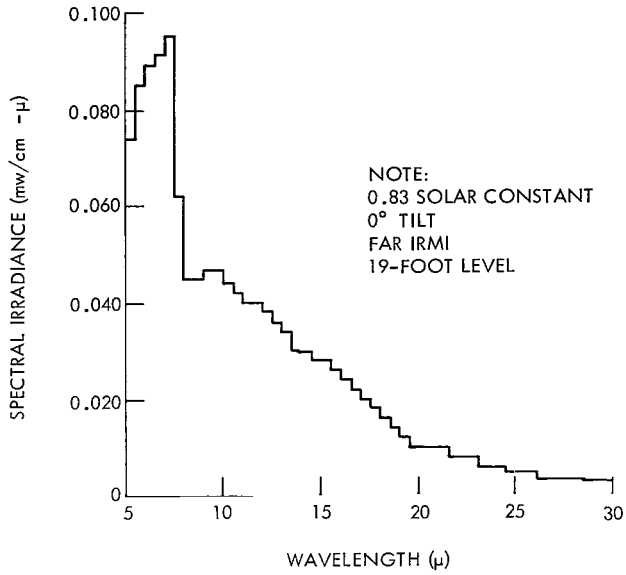

Figure 17—Spectral irradiance under module 107.

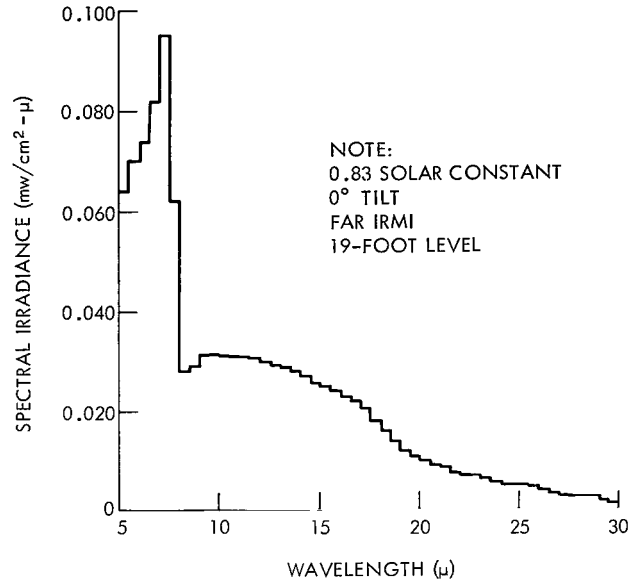

Figure 18—Spectral irradiance under module 32.

frequencies but was reduced to only the points needed to describe the continuum after the absence of absorption bands was noted. The spectra of Figures 16 to 19 constitute the basic spectral irradiance model of the solar array limited to the 0.0346 steradian field of view of the instrument. The spectrum to be used for a unit test item is discussed further below.

Solar-off Condition

The instruments were positioned at the 31-foot level and the solar simulator was turned off to determine the possible extraneous sources of energy and to gain a higher confidence factor as to the direction of the differential radiance of the instruments. Two-minute data-taking intervals were made every 10 minutes for the 1-hour cool-down condition, with the shutter being placed over the instruments between intervals in order to maintain constant instrument temperatures. The line at 3.35μ of the far IRMI, and the bands at 3.35, 2.36, 2.12, and 1.7μ of the near IRMI, did not appear for the first 2-minute data interval after the solar simulator was turned off. The source of the energy then must be the arc-electrode-bulb complex for this particular grouping of lines. The amplitude spectra shown in Figure 20 for the far IRMI shows the disappearance of the 3.35μ line. The dot-dash curve is the

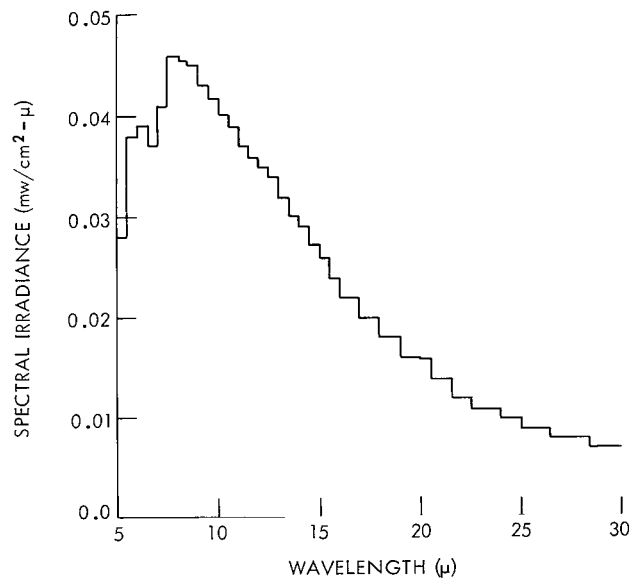

Figure 19—Spectral irradiance under module 32 at high tilt angle.

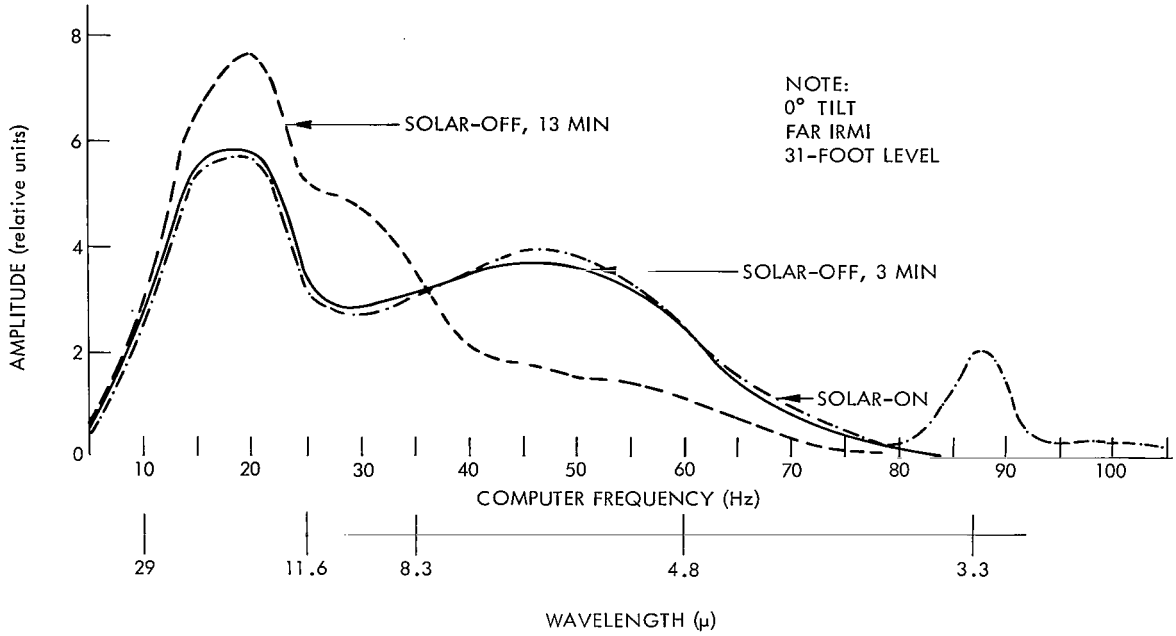

Figure 20—Amplitude spectra under module 64, solar-off condition.

spectrum just before the solar simulator was extinguished, while the solid curve is the first spectrum taken after solar-off. There is some evidence of slight cooling throughout the spectral range; however, the most dominant difference is the disappearance of the band in the 3.35μ region. The dashed curve is the amplitude spectrum 13 minutes after the solar-off. The amplitudes of the frequencies below 35 are seen to be increasing with time while those above 35 decrease. The net flow of energy is into the instrument at high frequencies; this reverses at frequencies below 35. The foregoing information was needed for this particular experiment because of the marginal information gained from the phase angle data of the computer reduction method.

Total Irradiance

The irradiance values were determined by integrating the areas under the spectral irradiance curves. A summary of the results is given in Table 2 for the spectral range 5.0 to 29.3μ and in Table 3 for the spectral range 2.9 to 5.0μ. The units for the energy values are mw/cm^2 as received by the instrument, which has a half-angle of acceptance of 6.0 degrees. The information listed in column A is the particular module under which the instruments were located and at the given distance from the mean height of the optics (e.g., 19-, 25-, or 31-foot levels). Module 64 is centrally located so that the tilt directions were specified according to compass directions as shown in Figure 21. Modules 32 and 107 are located nearer to the edges of the array, and the tilt directions are also shown in Figure 21.

The zero degree or normal direction used during the measurements was that of the normal direction of the front window of the instruments. The skewness of the optical axis of the Michelson

Table 2

Total Irradiance 5.0 to 29.3μ Region in Terms of Instrument Field of View.

Column A	Mean Height from Optics (feet)	Tilt Angle (degrees)										
		-20	-15	-10	-5	-2.5	0	2.5	5	10	15	20
				Northwest					Southeast			
Mod 32	19			0.44	1.22	1.22	1.18	0.76	0.68	0.51	0.51	
	25			0.40	1.30	1.30	1.13	0.88	0.62	0.39		
	31						1.02		0.43	0.43	0.47	0.42
				Northeast					Southwest			
Mod 107	19			0.42	1.35	1.50	1.38	1.25	0.71	0.53	0.53	
	25			0.37	1.35	1.45	1.50	0.96	0.80	0.42	0.42	
	31						1.25		0.39	0.46	0.52	0.46
				North					South			
Mod 64	19			0.39	1.08	1.08	1.17	0.50	0.50	0.54		
	25						1.27					
	31			0.37			1.26		0.40	0.64		
				East					West			
Mod 64	19	0.34		(0.17)	1.52	1.40	1.17	1.07	0.41	0.54	0.58	
	25			0.35	1.38	1.40	1.27	1.08	(0.22)	0.42		
	31			0.35	1.21		1.26		0.28	0.30		

Table 3

Total Irradiance 2.9 to 5.0μ Region in Terms of Instrument Field of View.

Column A	Mean Height from Optics (feet)	Tilt Angle (degrees)				
		-5	-2.5	0	2.5	5
		Northwest			Southeast	
Mod 32	19	.41	.26	.25	.22	.21
	25	.16	.23	.26	.25	.26
	31			.23		.23
		Northeast			Southwest	
Mod 107	19		.23	.24	.23	.20
	25		.28	.23	.20	.19
	31			.16		.12
		North			South	
Mod 64	19	.25	.23	.22	.25	.3
	25			.20		
	31		.16	.18		.16
		East			West	
	19	.24	.28	.22	.22	.21
	25	.22	.20	.20	.18	.19
	31		.14	.18		.16

cube, with respect to the geometric normal of the instrument casing, causes the asymmetry of the results given in the tables.

The data presented in Tables 2 and 3 are in terms of the field of view of the instruments. The energy incident onto a unit test item, positioned in the test volume at some arbitrary tilt angle to the normal, depends on the view of the solar array by the test item. Therefore, the more useful form of the data is in terms of the solid angle of the solar array at the various distances from the mean height of the solar array. To present the data in terms of the solid angle of the solar array, it is necessary to interpret the data with respect to the nature of the radiation field, i.e., the dependence of the energy values as a function of tilt angle with respect to the normal. The data of Table 2 are plotted in Figure 22 as a typical spatial distribution. The figure shows that the measured energy values have a strong dependence on angle at the small tilt angles, and at the larger tilt angles the measured energy values become essentially independent of angle. A Lambertian surface, or perfectly diffuse surface, is one that emits radiation in all directions in an amount proportional to its projected area (Reference 5); therefore, a radiation detector would measure the same amount of energy independent of the tilt angle. Within the small range of angles of the experiment, the data exhibit a similar property (an independence of energy with tilt angle so that at the larger tilt angles the radiation field can be characterized as being diffuse, at least to a first approximation). The data at the smaller tilt angles are those typically produced with an instrument positioned in a "collimated" beam of radiation. By considering the angular response of the instrument of Figure 11, and postulating a "collimated" beam with a decollimation half angle of 3.5°, data similar to Figure 22 can be obtained. Therefore, the radiation field can be described as being composed of a "collimated" beam and a "diffuse" field.

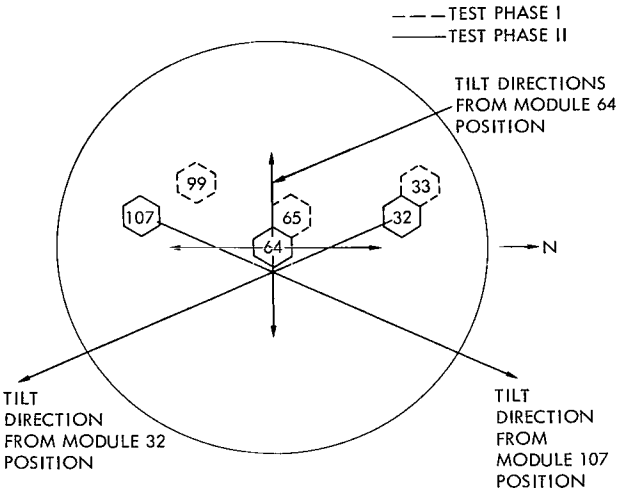

Figure 21—Tilt directions of interferometers.

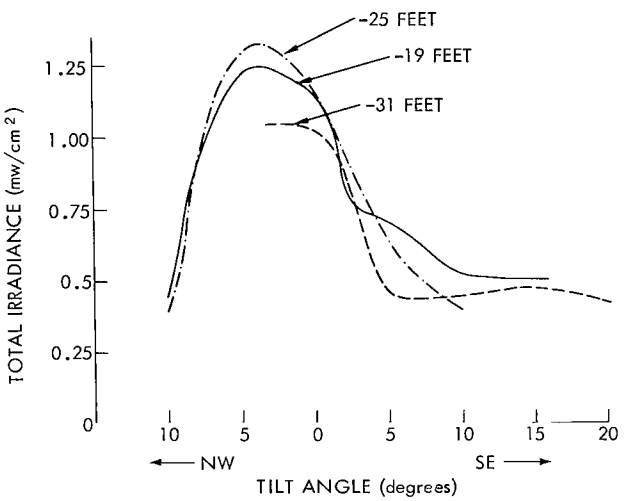

Figure 22—Spatial distribution under module 32.

In order to arrive at an estimate of the energy being received by a unit test area that views the entire array from the position of the instruments, the numerical average of the diffuse component was taken at the various locations of the instruments of Table 2 and resummarized in Table 4.

Table 4

Energy Incident Onto a Test Item Viewing the Entire Solar Array.

Location of Test Item	Height Position in Chamber (feet)	Average Diffuse Component of Irradiance (mw/cm^2)	Solid Angle Viewed by Test Item Ω_{SES} (sr)	Total Diffuse Component E_{SES} on Test Item (mw/cm^2)	Average Collimated Component of Irradiance (mw/cm^2)
Under Mod 32	19	.54	.755	11.9	.94
	25	.47	.456	6.18	1.09
	31	.44	.303	3.85	.84
Under Mod 107	19	.49	.755	10.7	1.25
	25	.43	.456	5.65	1.25
	31	.46	.303	4.04	1.00
Under Mod 64	19	.48	.845	12.2	1.30
	25	.38	.492	5.83	1.25
	31	.38	.318	3.72	1.01
		A	B	C	D

The solid angles subtended by the solar array at the instrument locations were computed on the basis of the projected area of one parabola times the 127 modules at the mean heights of 19, and 31 feet, and are listed in Table 4 as Ω_{SES}. The ratio of Ω_{SES} to the solid angle of the far IR instrument, times the energy values of column A, was used to estimate the total diffuse component incident onto the unit test area; the results are in column C.

The collimated portion was estimated by subtracting the "average" diffuse component from the total value at the various positions of the far IR instrument. The maximum value of the near IR instrument was added to this value, and the results are listed in column D of Table 4. The energy incident onto a test item that views the entire array is thus the sum of columns C and D. These values represent the basic model for the infrared energy in the chamber when the solar simulator is operated at 116 mw/cm^2 of direct solar energy (0.28 to 2.5μ), and there is no test item in the chamber.

Thus the corresponding spectral irradiance curve to be used must be weighted according to the energy values of column C and D of Table 4. If the data are to be used for estimating purposes, a suggested procedure is to average numerically Figures 16 to 18, the results of which thus correspond to an average collimated portion (column D) plus 0.0346 sr of the diffuse component. The composite spectrum incident onto the unit test item is thus weighted more heavily for the diffuse component of Figure 19 (as seen from column D of Table 4).

Variations of Basic Infrared Model Caused by Changing of Chamber Parameters

The measurements made while the spacecraft model was positioned in the SES were at normal incidence only; i.e., the gimbal available for phase II was not ready for the phase I program so that the instruments were always looking straight up at the solar array. The information gained from this phase is summarized in Table 5. As explained under "Energy Calibration," it was not possible to obtain a calibration for the near IRMI instrument for wavelengths shorter than 2.9μ. The data displaying the more drastic change as a function of the experimental parameters were the near IRMI and not the far IRMI. Nevertheless, some knowledge of the changes in the radiation field when the parameters are changed can be obtained by comparing the amplitude voltages on the Fourier transform for the instruments.

The data listed in column A of Table 5 are the Fourier amplitudes at the given computer frequencies corresponding to the wavelengths of column B. The frequencies chosen are those of the lines being emitted by the arc, as well as the peak of the infrared energy originating at the lamp complex. The spacecraft model position is designated according to Figure 4 where the 90°W position is the dotted outline and the 0° position the solid line. The module that should be most affected by the model orientation is 65; modules 33 and 99 should be less affected since they are located farther from the tilt axis. This is assuming that any measured change would be caused by re-reflections direct to the instruments as compared to reflections to the array, subsequent heating of the array, and thence to the measuring instruments.

Table 5

Total Irradiance in SES as a Function of Spacecraft Tilt Angle and Solar Intensity.

		Module 33				Module 65				Module 99			
Computer Frequency Column A	Wavelength (microns) B	0.85sc[1]	0.65sc			0.85sc	0.65sc			0.85sc	0.65sc		
		85°[2] C	85° D	55° E	0° F	85° G	85° H	55° I	0° J	85° K	85° L	55° M	0° N
164	1.69	10.6	3.83	3.13	2.97	7.74	3.63	2.54	2.50	8.85	3.67	3.29	2.87
128	2.12	5.30	1.50	1.25	1.50	4.50	1.15	1.70	1.40	4.05	1.83	1.80	1.55
115	2.36	9.40	3.40	2.90	2.97	7.30	2.08	2.54	2.55	7.10	3.15	2.80	2.55
83	3.35	3.10	1.39	1.10	1.20	1.94	1.00	1.00	0.80	2.20	0.95	0.80	0.86
37	8.0	1.05	0.36	0.36	0.28	0.62	0.36	0.20	0.20	0.66	0.20	0.24	0.28
Total Far IR Energy		1.60	1.54	1.53	1.53	1.54	-	-	1.49	1.50	-	-	-

[1]sc ≡ solar constant
[2]tilt angle of space vehicle

The change of the energy in the beam from 116 mw/cm^2 (0.83 sc) to 91 mw/cm^2 (0.65 sc) produced the most drastic change for the near IR instrument and a relatively small change for the far IR instrument. The magnitude of the change for the given frequencies was totally unexpected; there is no explanation for this at the present time. The change in total incident energy was 22 percent, whereas the indicated change for the lines is in the order of 50 to 75 percent. At the high frequencies listed, the instrument radiance is very small or negligible; the areas under the amplitude spectra for the 0.83 sc vs the 0.65 sc conditions should be directly relatable to that obtained from a reduced energy spectra. That the measured change in the lines given in Table 5 was 50 to 75 percent, whereas, it should have been on the order of 20 to 25 percent, cannot be explained. The last row in each of the columns for the various conditions is the total energy as measured by the far IR instrument. The change in the energy of the solar beam results in a small change in the total far IR energy measured in the test volume. After the solar beam was changed from 0.83 to 0.65 sc, 5 hours elapsed before the beginning of measurements at 0.65 sc. The measured temperatures of the solar array had stabilized by this time so that the 4 percent decrease should be representative of the far IR energy change for the two conditions. The spacecraft model orientation has little or no effect on the measured values as shown in Table 5 for either the near or far IR instruments. The variation shown is most likely caused by positional errors of the instruments. That is, the solar beam is non-uniform and any energy measurements that are made must account for very precise location of the instruments with respect to the beam at the shorter wavelengths. However, the measurement program does indicate little or insignificant interchange between the given test item and the solar array.

The data obtained, with and without the spacecraft model in the chamber, are inconclusive. The effect on the IR energy caused by adding a large reflecting surface in the solar beam cannot be determined. The positions of the instruments were not identical for phases I and II of the measurement program, and the measured change can be attributed to either the change of position or to the addition of the large reflecting surface. Figure 23 is the typical spectral irradiance curve with the spacecraft model in the chamber; it has characteristics corresponding to high energy values obtained without the model in the chamber, as shown in Figure 17.

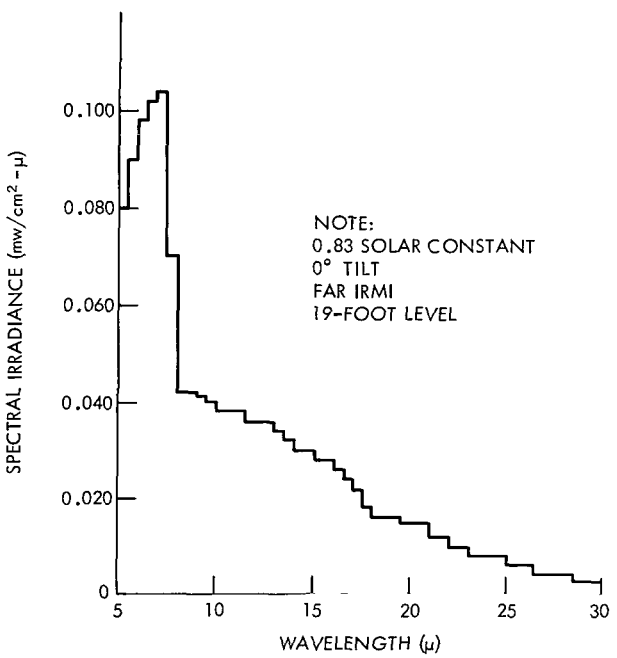

Figure 23—Spectral irradiance under module 33 with spacecraft model in chamber.

CONCLUSIONS AND RECOMMENDATIONS

The above study has been carried out to define an IR model of the solar array to be used

when the IR energy affects test item temperatures. To this end the following results have been achieved for the basic model of the IR energy:

(1) The spectral irradiance has been defined for IR energy from 2.9 to 29.3μ.

(2) The total irradiance has been defined for a test item viewing the entire solar array at various heights and positions in the direct solar beam. The results are summarized in Table 4.

(3) The spectral irradiance has been defined for a test item viewing the entire solar array at various heights and positions in the direct solar beam. The collimated portion can be estimated using the data in Figures 16 to 18, which include 0.0346 sr of the diffuse component. The diffuse spectral irradiance is that of Figure 19. The composite spectrum incident onto the unit test item is thus the weighted average (according to columns C and D of Table 4) of the diffuse and collimated spectra.

(4) The variations to the basic IR model due to changing the mode of operation of the chamber were as follows:

a. Lowering the direct solar intensity from 116 to 91 mw/cm^2 (a 22-percent change) caused a 4-percent decrease in the energy as measured by the far IR instrument aimed directly into the beam.

b. Changing the orientation of the OAO thermal model resulted in no measurable change in the far IR energy as measured by the instrument aimed directly into the beam; however, the near IR instrument may have indicated trends dependent in spacecraft orientation.

(5) Information on the effect on the basic IR model by the introduction of a large reflecting surface in the direct solar beam is inconclusive. One opinion is that if the reflecting surface were to affect the IR energy, a change in the IR would be expected when the reflecting surface is tilted with respect to the optic axis of the solar beam. Since no measurable change in the energy values was observed, it may be concluded that the introduction of the surface caused little or no effect on the IR energy.

The infrared radiation in the SES should be studied more completely to better define the IR model. The IR studies should begin with thorough measurements of the individual mercury-xenon lamps to better define the short wavelength variations of spectral irradiance as a function of lamp input power. The interferometers should be modified to prevent the energy reversals presently encountered, thus enabling automatic data reduction to be employed. Given such an automatic system, the instruments should be employed routinely (whenever the solar simulator is used for test purposes) to gain further knowledge of IR energy as a function of changing test parameters.

Goddard Space Flight Center
National Aeronautics and Space Administration
Greenbelt, Maryland, September 13, 1968
124-09-19-08-51

REFERENCES

1. Caruso, Paul S., "Orbiting Astronomical Observatory Integrated Spacecraft Test Program: α/ϵ Heater Skin Test Report," Goddard Space Flight Center, DIRS No. 01048 January 1968.

2. Longhurst, R. S., "Geometrical and Physical Optics," London: Longmans, Green and Co. Ltd., 1960.

3. Connes, Janine, "Spectroscopic Studies Using Fourier Transformations," ASTIA Report 409 869, January 1963.

4. Villasenor, Anthony J., "Digital Spectral Analysis," NASA Goddard Space Flight Center Technical Note D-4510, June 1968.

5. Strong, John, "Concepts of Classical Optics," San Francisco: Freeman and Company, 1958.

Appendix A

Nomenclature

α = Solar absorptance

ϵ = Thermal emittance

γ = Angle from normal direction of I_0

μ = Microns = 10^{-4} cm

ν = Frequency

$B(\nu)$ = Incident spectrum

I_0 = Incident radiation

IR = Infrared

MI = Michelson interferometer

sr = Steradian

x = Path difference = twice the mirror displacement

Appendix B

Tolerances

The tolerances assigned to the spectral irradiance and total irradiance are caused by many factors. These include errors in determining the responsivity, detector irradiance, and signal voltages—all at a given wavelength. One problem in determining a tolerance is the difficulty in arriving at values for the various parameters that are mutually independent of each other. The end result most probably contains errors included more than once; however, the results do give relative magnitudes of the expected error.

The data to be used include the responsivity of the instrument calculated from the calibration data taken with the black body source at 10°, 50°, and 95°C. The detector irradiance, $N_{\nu B}$, and the signal amplitude, V, are taken from the data obtained with the instruments viewing the liquid nitrogen walls. These data are then used to calculate the energy from the black body source at 150°C and are as given in Table B1. The handbook values of the energy from the black body source are similarly listed in Table B1. The difference between the two sets is used as an estimate of the expected error for the spectral irradiance values. The square root of the sum of the squares was used to estimate the expected error for the total irradiance; the value was ±7.0 percent.

Table B1

Tolerances for Spectral Irradiance.

Wavelength λ (microns)	Responsivity Re_{ν} (volts-cm^2-μ/mw)	Detector Radiance $N_{\nu B}$ (mw/cm^2-μ)	Signal Level V (volts)	Calculated Energy E (mw/cm^2-μ)	Handbook Value of Energy E_{BB} (mw/cm^2-μ)	Error (%)
29.2	33.2	1.2	36	2.30	2.54	-9.5
23.9	22.2	2.3	70	5.40	4.85	11.0
20.2	18.2	3.6	96	8.90	8.08	10.1
14.6	15.6	6.8	210	20.3	19.4	4.6
13.2	15.0	7.7	258	24.9	24.5	1.6
10.9	10.0	9.2	306	29.8	35.8	11.2
9.0	8.3	10.0	330	50.0	47.2	6.0
8.6	7.7	10.0	336	54.0	49.6	8.8
7.3	7.7	9.5	372	58.0	55.1	5.3
6.4	7.7	7.0	366	59.5	55.0	8.2
5.7	7.0	5.8	312	50.8	51.0	0.40
5.1	7.2	4.0	256	39.0	44.0	-13.0

NASA-Langley, 1969 —— 29

NATIONAL AERONAUTICS AND SPACE ADMINISTRATION
WASHINGTON, D. C. 20546

OFFICIAL BUSINESS

FIRST CLASS MAIL

POSTAGE AND FEES PAID
NATIONAL AERONAUTICS AND
SPACE ADMINISTRATION

02U 001 36 51 3DS 69134 00903
AIR FORCE WEAPONS LABORATORY/AFWL/
KIRTLAND AIR FORCE BASE, NEW MEXICO 8711

ATT E. LOU BOWMAN, ACTING CHIEF TECH. LI

POSTMASTER: If Undeliverable (Section 158 Postal Manual) Do Not Return

"The aeronautical and space activities of the United States shall be conducted so as to contribute . . . to the expansion of human knowledge of phenomena in the atmosphere and space. The Administration shall provide for the widest practicable and appropriate dissemination of information concerning its activities and the results thereof."

—NATIONAL AERONAUTICS AND SPACE ACT OF 1958

NASA SCIENTIFIC AND TECHNICAL PUBLICATIONS

TECHNICAL REPORTS: Scientific and technical information considered important, complete, and a lasting contribution to existing knowledge.

TECHNICAL NOTES: Information less broad in scope but nevertheless of importance as a contribution to existing knowledge.

TECHNICAL MEMORANDUMS: Information receiving limited distribution because of preliminary data, security classification, or other reasons.

CONTRACTOR REPORTS: Scientific and technical information generated under a NASA contract or grant and considered an important contribution to existing knowledge.

TECHNICAL TRANSLATIONS: Information published in a foreign language considered to merit NASA distribution in English.

SPECIAL PUBLICATIONS: Information derived from or of value to NASA activities. Publications include conference proceedings, monographs, data compilations, handbooks, sourcebooks, and special bibliographies.

TECHNOLOGY UTILIZATION PUBLICATIONS: Information on technology used by NASA that may be of particular interest in commercial and other non-aerospace applications. Publications include Tech Briefs, Technology Utilization Reports and Notes, and Technology Surveys.

Details on the availability of these publications may be obtained from:

SCIENTIFIC AND TECHNICAL INFORMATION DIVISION

NATIONAL AERONAUTICS AND SPACE ADMINISTRATION

Washington, D.C. 20546